Available online at www.sciencedirect.com
SCIENCE DIRECT®
Cement & Concrete Composites 28 (2006) 102–114
Cement & Concrete Composites
www.elsevier.com/locate/cemconcomp

Sensitivity analysis of reinforced concrete beams strengthened with FRP laminates

Carlos A. Coronado [a,1], Maria M. Lopez [b,*]

[a] Department of Civil and Environmental Engineering, The Pennsylvania State University, 3127 Research Drive CATO Park, Room 117, State College, PA 16801, USA
[b] Department of Civil and Environmental Engineering, The Pennsylvania State University, 212 Sackett Building, University Park, State College, PA 16802-1408, USA

Received 13 July 2004; accepted 19 July 2005
Available online 20 October 2005

Abstract

Numerical procedures are proposed to predict the failure of reinforced concrete (RC) beams strengthened in flexure with fiber-reinforced polymeric (FRP) laminates. The framework of damage mechanics was used during the modeling. Numerical results were validated against experimental data obtained from 19 beams strengthened with different types of FRP. These beams failed by concrete crushing, cover failure and plate debonding. The numerical models were capable of predicting the experimentally observed load–deflection, failure load and failure modes. The sensitivity of the numerical results was studied. In particular, the effect of the concrete constitutive behavior and different modeling considerations was evaluated. It was found that the fracture energy of the concrete–repair interface plays a central part in predicting plate-debonding failures.

Keywords: Composite materials; Fracture energy; Finite element modeling; Damage mechanics; Debonding; Numerical modeling; FRP laminate; Reinforced concrete beam

1. Introduction

Strengthening reinforced concrete (RC) beams with fiber-reinforced polymer (FRP) composites is becoming an attractive alternative for the construction industry. These laminates offer all the advantages of composite materials, such as a low volume to weight ratio, and a high strength-to-weight ratio. Experimental tests of FRP-strengthened beams have identified a number of possible failure modes: tensile rupture of the composite laminate, debonding failure between the FRP laminate and the concrete substrate, concrete cover failure, and concrete crushing [1]. Although experimental data is valuable in understanding the behavior of this strengthening system, analytical and numerical solutions are needed to further comprehend and predict the behavior and failure mechanism of the strengthened beams.

Numerical modeling of FRP-strengthened beams represents a formidable challenge because other aspects—such as loading sequence, construction procedure, nonlinear material behavior, crack propagation and residual stresses—may have a significant impact on the results obtained in such an approach. Different modeling approaches, partially incorporating these aspects, have been proposed up to now; but sensitivity analyses are needed in order to identify the principal parameters controlling the numerical response of FRP-strengthened beams and to simplify the modeling procedures currently available.

Among different modeling approaches proposed to date, Ziraba and Baluch [2] presented a nonlinear finite-element code to simulate the global behavior, up to failure, of RC

* Corresponding author. Tel.: +1 814 8659423; fax: +1 814 8637304.
E-mail addresses: cac1052@psu.edu (C.A. Coronado), mmlopez@engr.psu.edu (M.M. Lopez).
[1] Tel.: +1 814 8659675; fax: +1 814 8659668.

0958-9465/$ - see front matter © 2005 Elsevier Ltd. All rights reserved.
doi:10.1016/j.cemconcomp.2005.07.005

beams externally reinforced. They were able to predict the behavior of strengthened members subjected to arbitrary load histories previous to strengthening. In this approach, the interfacial behavior between concrete and the internal and the external reinforcement was modeled using six-node interface elements; nine-node Lagrangian elements were used for modeling the concrete and external laminate, whereas a three-node element represented the internal reinforcement. Arduini et al. [3] conducted a finite-element analysis of eight FRP-strengthened beams using the commercial code ABAQUS. During this study, the concrete was modeled using the smeared crack approach, and a perfect bond was assumed between the FRP and the concrete. This analysis was limited to beams with a monotonic loading history and without damage prior to FRP installation. Wong and Vecchio [4] used link and contact elements following linear and elastoplastic bond laws in order to model the bond-slip behavior at the bond interface of FRP-strengthened beams. A two-dimensional nonlinear finite-element code based on the Modified Compression Field Theory was used during the analyses. The procedure was able to predict the load–deflection behavior of FRP-strengthened beams failing by laminate debonding only when using an elastoplastic bond-slip behavior. However, the authors stated that a more clearly defined constitutive relationship for the bond elements must be developed to further improve and validate the model capability.

From these previous studies, it can be concluded that due to the challenges faced during the numerical analysis of FRP-strengthened beams, most of the research in this area has been devoted to improving the modeling techniques. From a practical point of view, it is also necessary to identify the principal material properties affecting the outcome of the numerical simulations; evaluate the sensitivity of the numerical results to variations in these material properties; and to recommend procedures for estimating such properties when experimental data are not available. This study aims at fulfilling these needs.

For this purpose, numerical results were validated against experimental data obtained from 19 beams strengthened with different types of FRP, and their sensitivity to concrete constitutive behavior and different modeling considerations was evaluated. In addition, practical recommendations are given for the modeling of FRP, epoxy, selecting model parameters and element size.

2. Experimental program

Experimental data was obtained from a previous research project [5] and from the literature review [6]. A total of 19 beams, strengthened with different FRP types, were selected for comparison with the numerical results. These beams failed by concrete crushing, cover failure, and/or plate debonding.

Series A corresponds to three large-scale beams tested by Benkert [5]. Geometric properties of these specimens are described in Table 1. The beams were tested under four-point bending. Beam A2 was used as a control specimen, whereas beams A1 and A3 were strengthened with two plies of Carbon FRP of different lengths. Material

Table 1
Experimental database

Series specimens	Width, height, length (mm)	FRP type	A_{FRP} (mm^2)	FRP length (mm)	Type of failure
Series A	305, 406, 4064				
A1		CFRP	83.8	3195	CC
A2		None	–	–	SY
A3		CFRP	83.8	3500	CC
Series B	200, 150, 2300				SY
B1		None	–	–	SY
B2		None	–	–	C/P
B3		CFRP	60	2100	C/P
B4		CFRP	60	2100	C/P
B5		CFRP	180	2100	C/P
B6		CFRP	180	2100	C/P
B7		GFRP	270	2100	C/P
B8		GFRP	270	2100	
Series C	200, 150, 2300				
C1		None	–	–	CC
C2		None	–	–	CC
C3		CFRP	60	2100	CC/P
C4		CFRP	60	2100	CC/P
C5		CFRP	180	2100	CC/P
C6		CFRP	180	2100	CC/P
C7		GFRP	270	2100	CC/P
C8		GFRP	270	2100	CC/P

Note: CC = concrete crushing; SY = steel yield; C/P = cover failure followed by plate debonding; CC/P = concrete crushing followed by plate debonding.
Specimen details.

Table 2
Material properties for beams Series A (Benkert [5])

Properties	Concrete	Steel rebar	Steel stirrups	Epoxy	CFRP laminate
Modulus of elasticity, E (GPa)	36[a]	208.5	208.5	1.73	228
Yield strength, f_y (MPa)	–	523	489	–	–
Tensile strength, f_{tu} (MPa)	4.6[a]	703	725	23	3484
Compressive strength, f'_c (MPa)	58.6	–	–	–	–
Ultimate strain (%)	>0.3	17	17	2	1.7
Fracture energy (N/m)	146[a]	–	–		
Poisson's ratio	0.2[a]	–	–	0.36	0.26
Angle of dilatancy	20[a]				

[a] Determined using Eqs. (1)–(4), see Section 4. Determination of concrete parameters.

Table 3
Material properties for Series B and C (Rahimi [6])

Properties	Concrete	Steel rebar	Epoxy	GFRP laminate	CFRP laminate
Modulus of elasticity, E (GPa)	25	210	7	36	127
Yield strength, f_y (MPa)	–	575	–	–	–
Tensile strength, f_{tu} (MPa)	3	–	25	1074	1532
Compressive strength, f'_c (MPa)	58.6	–	70	–	–
Ultimate strain (%)	>0.3	>20	0.7	3.1	1.21
Fracture energy (N/m)	200	–	0.4	–	–
Poisson's ratio	0.2	0.3	0.3	0.3	0.3
Angle of dilatancy	20				

properties are presented in Table 2. Beams A1 and A3 failed by concrete crushing. Details of the testing program can be found from Benkert [5].

Series B and C correspond to 16 reinforced concrete beams tested by Rahimi and Hutchinson [6] under four-point bending. Beams B1, B2, C1, and C2 were used as control specimens. Geometric properties for these beams are presented in Table 1. Material properties are described in Table 3. Additional strengthening details can be obtained from Rahimi and Hutchinson [6].

3. Material constitutive behavior

3.1. Concrete model

A plastic-damage model is used in order to predict the constitutive behavior of concrete. In this approach, it is assumed that compressive crushing and tensile cracking are the main failure mechanisms of concrete. Both of these phenomena are the result of microcracking [7], which can be interpreted as a *local damage effect* controlled by a yield function, which defines their onset and evolution [8]. Particular details of the mathematical implementation of these ideas are given by Lubliner et al. [8] and Lee and Fenves [9]. The basic parameters required by this formulation are as follows:

1. The softening curve of concrete under uniaxial tension, as shown in Fig. 1, where f_t is the stress controlling the onset of microcracking; G_F is the total external energy supply, per unit of area, required to create, propagate, and fully break a Mode I crack in concrete; and w is the crack opening or separation.
2. The stress–strain curve of concrete under uniaxial compression, as shown in Fig. 2, where E_c is the modulus of elasticity; f_{co} is the *critical stress* ($f_{co} \sim 0.6 - 0.8f'_c$); which may be associated with the stress at which the volumetric strain reaches its maximum [8]; and f'_c is the compressive strength.
3. The Poisson's ratio of concrete (v_c) and angle of dilatancy (ψ). These parameters control the volume change of concrete in the elastic and inelastic regimes, respectively.

3.2. Steel model

The constitutive behavior of steel is predicted using an elastic perfectly plastic model, as described in Ref. [10]. In this approach, the steel behavior is elastic up to when the yield stress is reached. At this point, the material yields under constant load (Fig. 3). The parameters required by this formulation are the modulus of elasticity (E_s), Poisson's ratio (v) and yield stress (f_y).

3.3. FRP model

The behavior of FRP plates is predicted using a brittle cracking model, as described in Ref. [10]. In this approach, the FRP behavior is assumed to be linear up to when the failure strain (ε_u) is reached (Fig. 3). At this point, a crack develops and the material losses all its load-carrying

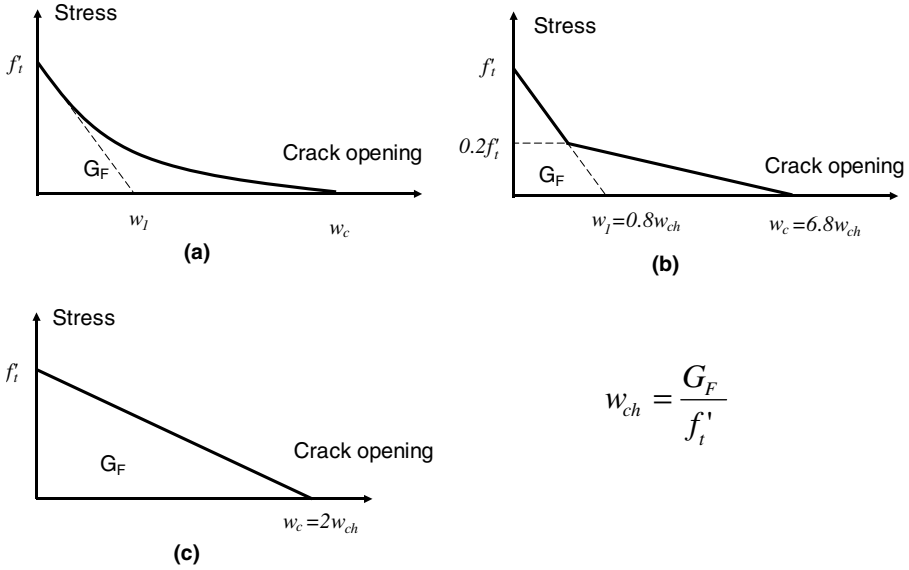

Fig. 1. Softening curve of concrete under uniaxial tension.

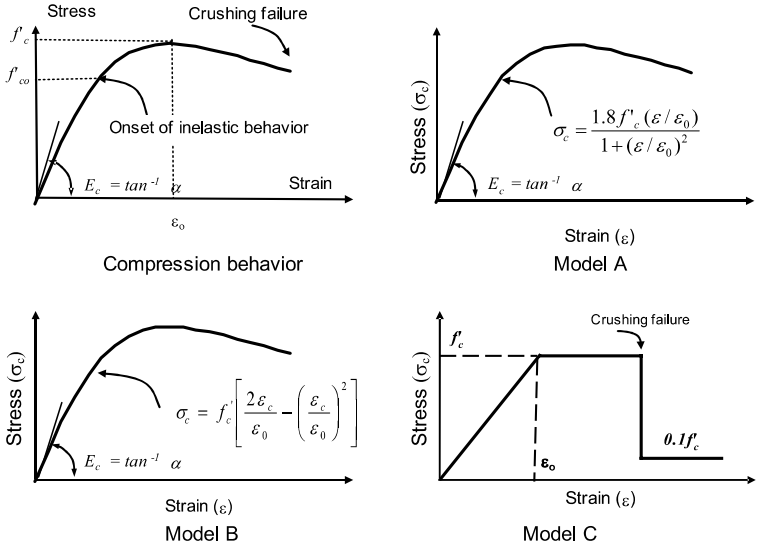

Fig. 2. Stress–strain behavior of concrete under uniaxial compression.

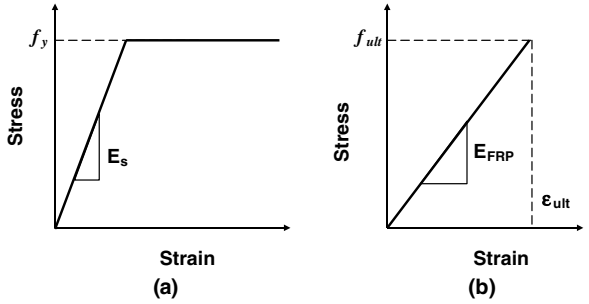

Fig. 3. Stress–strain behavior for steel and FRP laminate.

capacity. The parameters required by this formulation are the modulus of elasticity (E_{FRP}), Poisson's ratio (v) and failure strain (ε_u).

4. Determination of concrete parameters

As will be shown later, the behavior of RC beams strengthened with FRP is considerably influenced by the material properties of the concrete. However, this information may not be available to the designer. For that reason, this section is aimed to guide the selection of such parameters from basic properties such as the compressive strength, f'_c.

4.1. Softening curve

The softening curve for concrete can be determined experimentally, Ref. [11]. For example, the tensile strength, f_t, can be obtained from the splitting test results [12]; and

the fracture energy, G_F, can be calculated from the load deflection behavior of notched concrete beams [13,14]. However, if these experimental parameters are not available, alternative procedures are required.

The authors recommend estimating the concrete tensile strength, f_t (MPa), from Eq. (1) [15]; and the concrete fracture energy, G_F (N/m), using Eq. (2) [16], where f'_c (MPa) is the concrete compressive strength, w/c is the water cement ratio, d_a (mm) is the aggregate diameter, and $\alpha_0 = 1.44$ for crushed or angular aggregates. Once these parameters (f_t, G_F) have been determined, different analytical expressions can be used to approximate the softening curve [11]. For example, linear, bilinear or exponential functions can be employed to fit the shape of the curve. The authors recommend the bilinear approximation shown in Fig. 1(b).

$$f_t = 0.6\sqrt{f'_c} \tag{1}$$

$$G_F = 2.5\alpha_0\left(\frac{f'_c}{0.051}\right)^{0.46}\left(1+\frac{d_a}{11.27}\right)^{0.22}\left(\frac{w}{c}\right)^{-0.30} \tag{2}$$

4.2. Concrete stress–strain curve

If experimental data are not readily available [17], the authors suggest to estimate the concrete modulus of elasticity, E_c (MPa), using Eq. (3) [18], and the stress–strain behavior using model C from Fig. 2, where ε_0 is calculated according to Eq. (4) [15].

$$E_c = 4700\sqrt{f'_c} \tag{3}$$

$$\varepsilon_0 = 1.71\frac{f'_c}{E_c} \tag{4}$$

4.3. Parameters controlling volumetric change

The Poisson's ratio governs the volume changes of concrete for stresses below the critical stress level, f_{co}. The value of this parameter can be taken within the range of 0.15–0.2 [15]. After the *critical stress* level is reached, the concrete exhibits an increase in plastic volume under pressure [19]. The angle of *dilatancy* is the parameter used to model this behavior. Following Lubliner et al. [8] as a guideline and based on the sensitivity analysis presented in Section 6.5, an angle of *dilatancy* of 30° is recommended.

5. Finite-element models

The finite-element program ABAQUS [10] was used during the numerical analyses conducted in this study. In this section, several numerical simulations of RC beams, strengthened with FRP, are presented. They include specimens failing by concrete crushing, plate debonding and plate rupture. The typical finite-element mesh used during these simulations is shown in Fig. 4. The different element types used for constructing the finite-element models are listed in Table 4. Similarly, the material properties are presented in Tables 2 and 3.

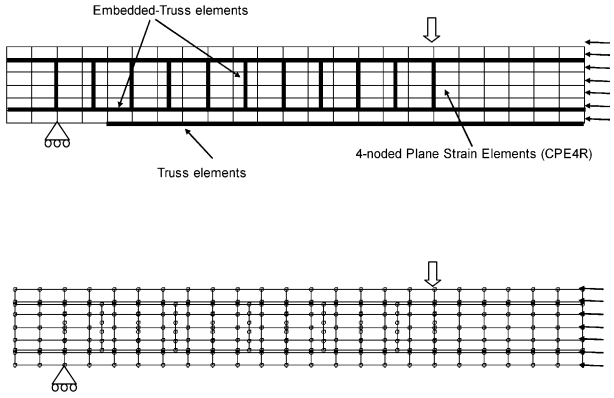

Fig. 4. Typical finite-element mesh.

Table 4
Finite-element types for numerical simulations

Material	Description	Code	Additional information
Concrete	Four-noded plain strain	CPE4R	Reduced integration
Steel	Two-noded truss	T2D2	Embedded
FRP	Two-noded truss	T2D2	–

5.1. Beams failing by concrete crushing

Numerical results obtained for 11 strengthened beams (including control beams) failing by concrete crushing are shown in Fig. 5. Results agree very well with those reported by Benkert [5] and Rahimi [6], with errors within 3–10% of the peak load. Good agreement between experimental and numerical results is also obtained for the entire load–deflection curves.

It is interesting to note that the simulations were extended beyond the load corresponding to concrete crushing. The numerical results indicate that plate-debonding failure follows the concrete crushing failure in all cases. After the plate-debonding failure, the beams retain a residual strength and ductility approximately equal to the bending capacity and ductility of the un-strengthened beams. This behavior agrees with that presented by Benkert [5] for beams A1 and A3. Experimental data for specimens C3–C8 was reported up to concrete crushing. The post-crushing behavior was not described in Ref. [6].

Numerical results predict plate-debonding failure of beam C5. However, this type of failure does not agree with that reported in Ref. [6]. Nevertheless, the predicted failure load is conservative. As shown later, the differences may be explained by taking into account the uncertainties in the values of fracture energy and tensile strength used during the simulations.

Predicted strain distributions for beam A1 are shown in Fig. 6(a). The strains were obtained at different locations within the CFRP plate, as shown in Fig. 6(b). As can be seen, the FEM simulation is very capable of capturing the experimentally observed strain trends and magnitudes for the entire loading range. These results confirm the validity of the finite-element models used in this study.

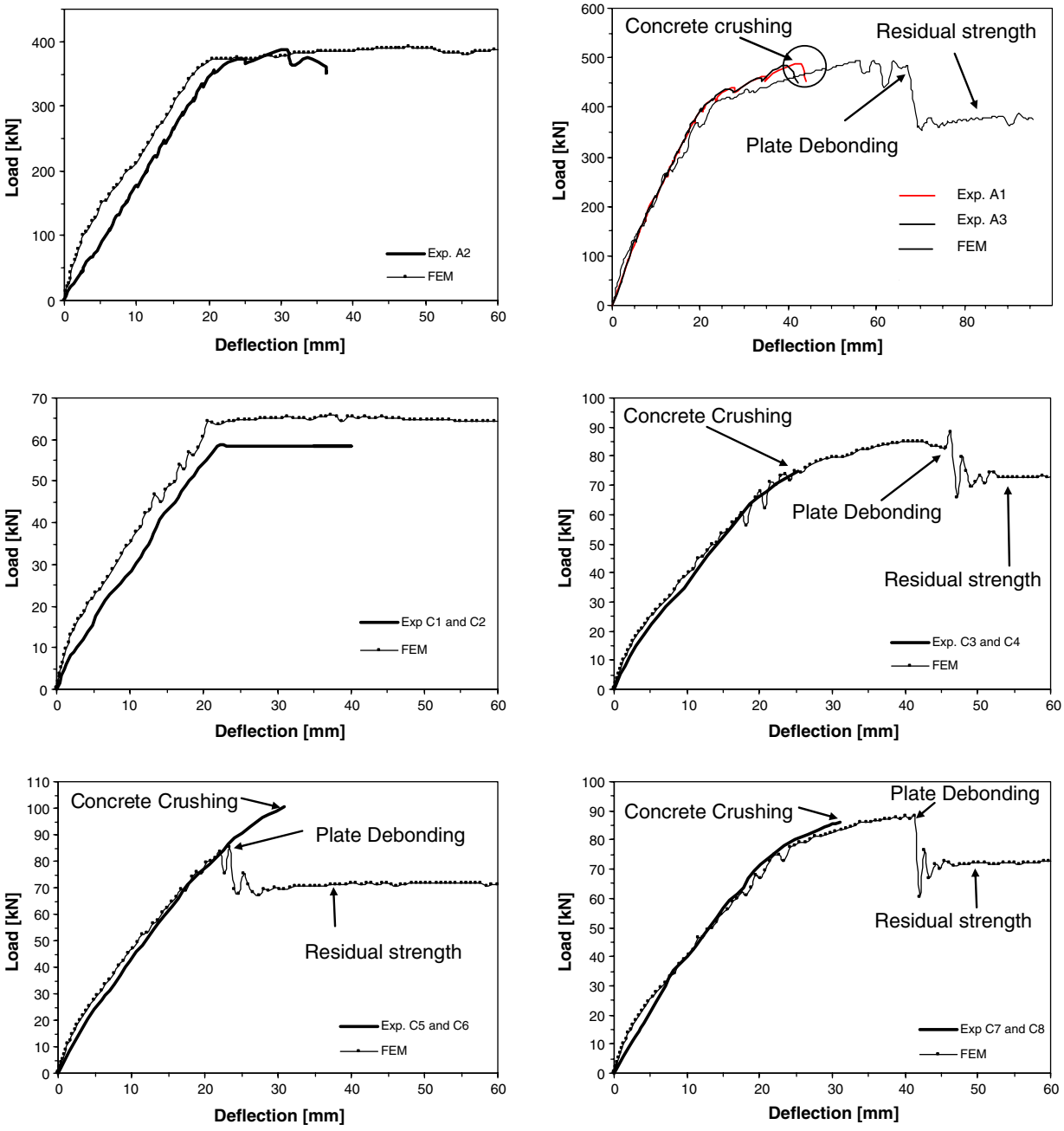

Fig. 5. Load–deflection behavior of strengthened beams failing by concrete crushing.

They are capable of predicting the global and local behavior of beams strengthened with FRP.

5.2. Beams failing by plate debonding

The framework of damage mechanics can be used for modeling and explaining the debonding failure of members strengthened with FRP. For instance, consider the FRP-strengthened beam shown in Fig. 7. Before any microcracking occurs, the beam's behavior is virtually elastic and no damage has taken place (i.e., the damage variable, d, is zero). Once the interfacial stresses reach a threshold-value (i.e., the tensile strength, f'_t, of the interface), microcracks start to form close to the concrete–epoxy interface. At this point, the damage of the interface starts to increase ($0 < d < 1$). Under further loading, the microcracks start to coalesce and macrocracks form. These macrocracks result in debonding of the FRP and total loss (damage) of the concrete–epoxy bond ($d = 1$).

Numerical results obtained for different beams failing by plate debonding are shown in Fig. 8. Results agree reasonably well with those reported by Rahimi [6], with peak loads consistently being under-predicted, within 10% of error. Good agreement between experimental and numerical results is also obtained for the load–deflection curves.

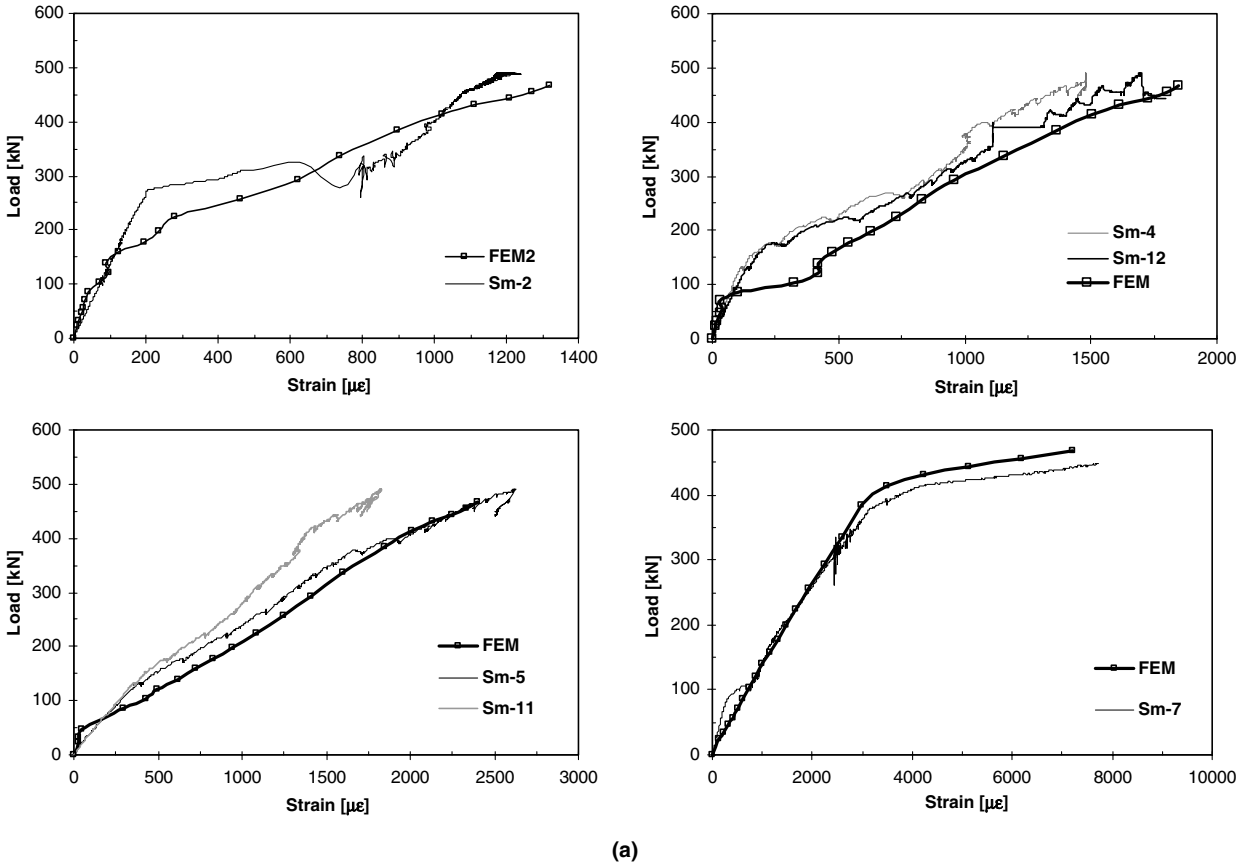

Fig. 6. (a) Predicted strain distributions for beam A1. (b) Strain gage layout.

Numerical results indicate that after the plate-debonding failure, the beams retain a residual strength and ductility approximately equal to the bending capacity and ductility of the un-strengthened beams. This behavior agrees with that reported by Naaman et al. [20].

5.3. Beams failing by plate rupture

Numerical simulations of beams failing by plate rupture are shown in Fig. 9. Beam B2 (Ref. [6]) was used as the control specimen. During the simulations, the area of CFRP reinforcement was varied in order to induce its tensile rupture. For this particular case, it was found that plate rupture occurs for areas of CFRP less than 20 mm^2. It was also noted that when the CFRP area is reduced, the rupture location shifts from the beam center towards one of the point loads. Therefore, in some of the simulations, the mid-span strain is lower than the CFRP failure strain (Fig. 9(b)). Numerical results also predict, that after the plate rupture, the beam retains its un-strengthened bending capacity, as shown in Fig. 9(a).

6. Sensitivity study

In this section, the sensitivity of the numerical solution was investigated with respect to concrete properties such

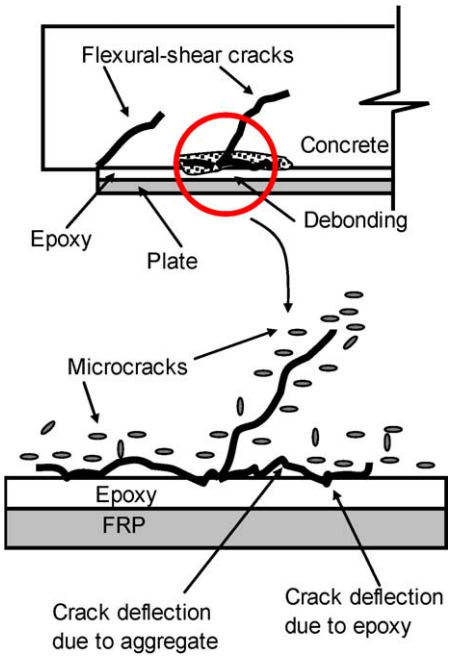

Fig. 7. Damage of the concrete–epoxy interface during debonding failure.

as tensile strength, fracture energy, tension softening, compression model and angle of dilatancy. Numerical results obtained for beams A1 and B3 are used in this section for illustration purposes. These beams were selected as control specimens since they failed by concrete crushing and plate debonding, respectively.

6.1. Sensitivity to tensile strength, f_t

The concrete tensile strength was changed from $0.5f_t$ to $2f_t$, where f_t is the tensile strength of the control specimens. It is interesting to note that several authors have proposed to use the concrete tensile strength as the limiting value for the interfacial stresses developed at the *concrete–epoxy interface* [21]. However, the numerical models were insensitive to this parameter alone, as shown in Fig. 10. The failure mode and peak load remained the same during the simulations. Beam A1 failed by concrete crushing followed by plate debonding; and beam B3 failed by plate debonding. The numerical results also indicate a slight increase in stiffness with the concrete tensile strength. However, from a practical point of view, such an increase is negligible.

It is important to point out the significance of these results. The concrete tensile strength cannot be used as the unique failure criterion for predicting FRP plate debonding. As will be shown later, the fracture energy of the concrete–epoxy interface plays a more important role in predicting this type of failure.

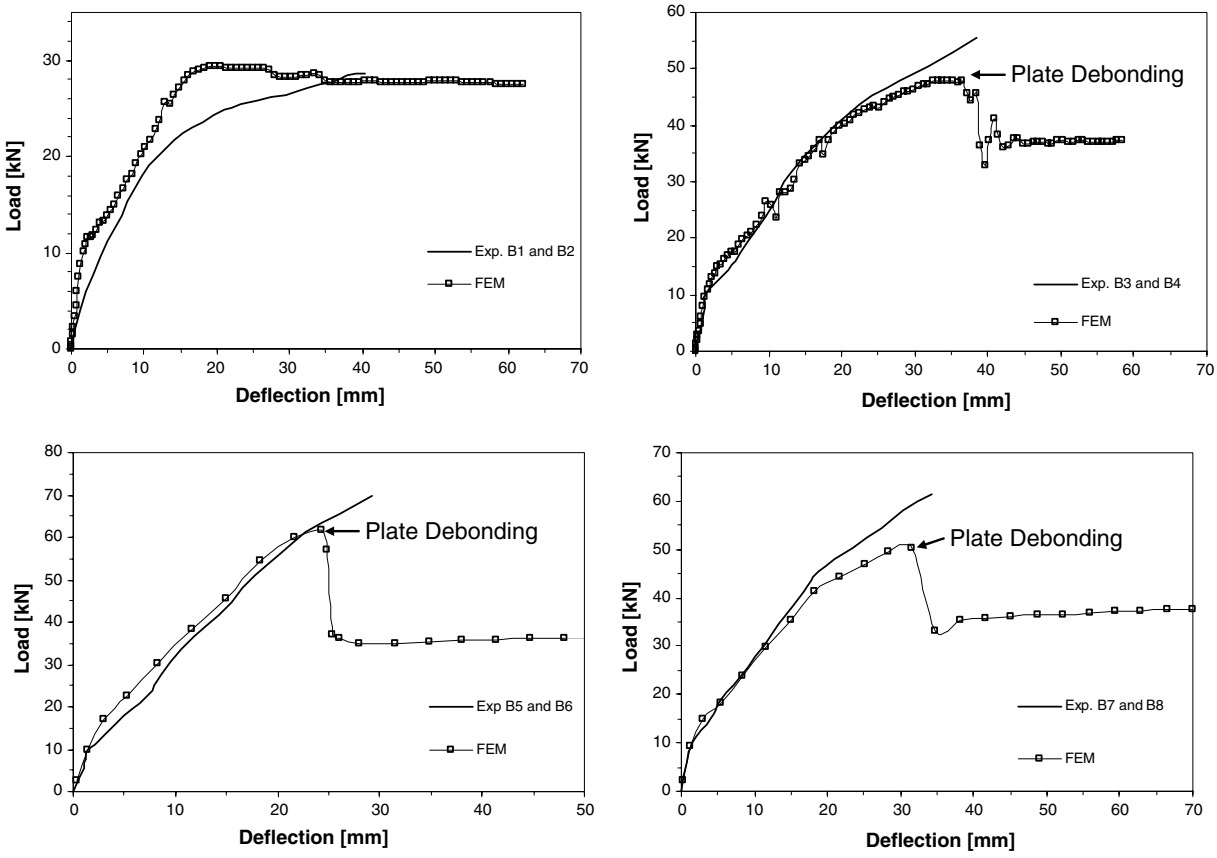

Fig. 8. Load–deflection behavior of strengthened beams failing by plate debonding.

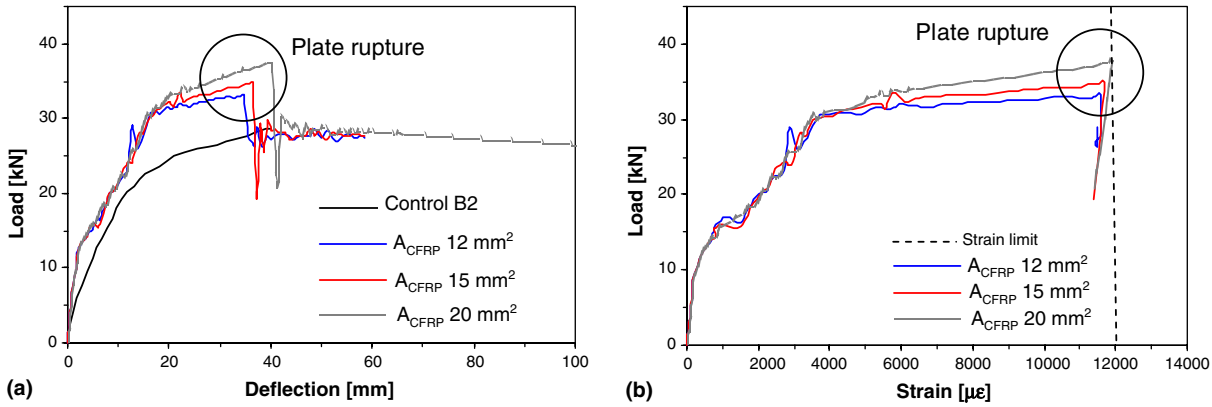

Fig. 9. Behavior of strengthened beams failing by plate rupture. (a) Load–deflection. (b) Load–midspan strain.

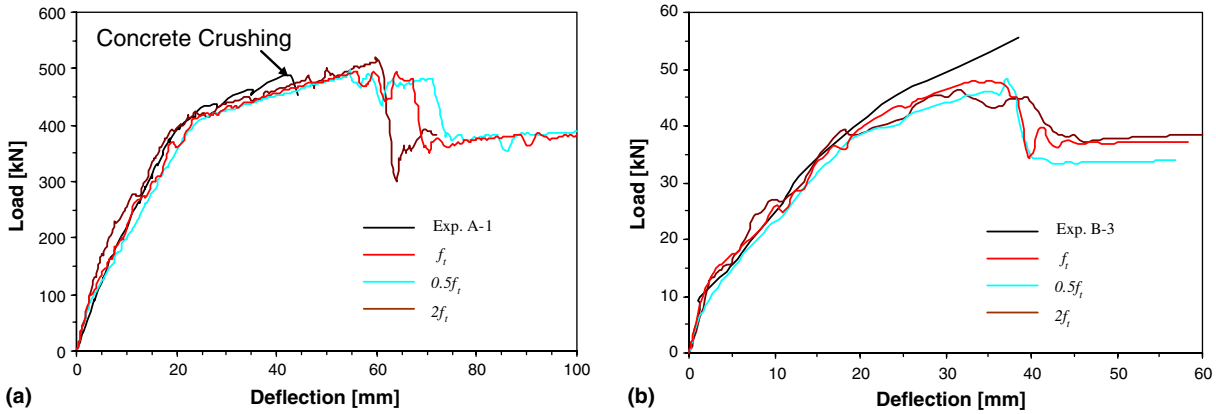

Fig. 10. Sensitivity to tensile strength.

6.2. Sensitivity to fracture energy

In this study, the concrete fracture energy was changed from $0.5G_F$ to $2G_F$, where G_F is the fracture energy of the control specimens. Numerical results shown in Fig. 11 indicate two important trends. Beam A1, failing by concrete crushing, is insensitive to changes in the concrete fracture energy. In contrast, the failure mode and peak load of beam B3, failing by plate debonding, are significantly affected by the magnitude of the concrete fracture energy. A low value of the concrete fracture energy ($0.5G_F$) results in premature plate debonding. Conversely, using a high value of concrete fracture energy ($2G_F$) results in a delay of the debonding failure and increase of the peak load.

Numerical results presented in this section indicate that concrete fracture energy, G_F, plays a significant role in predicting failures due to plate debonding. This finding agrees

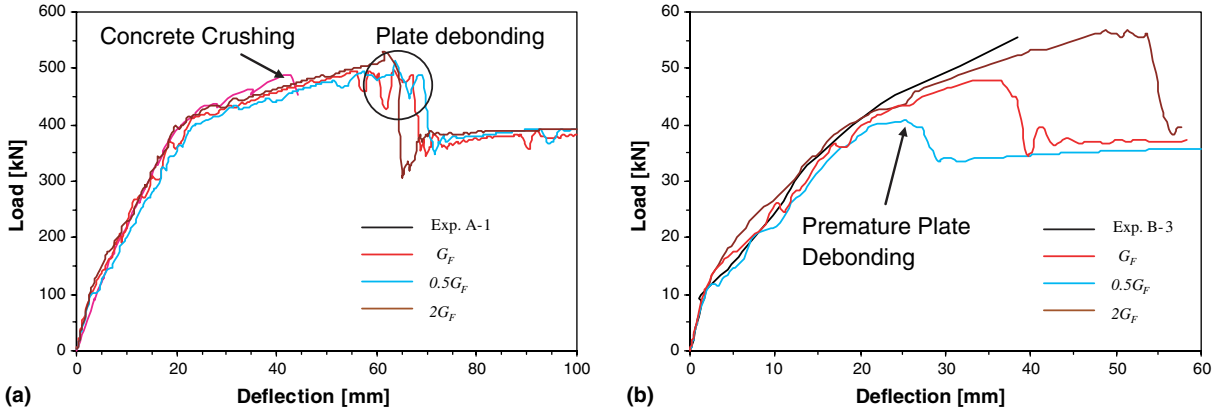

Fig. 11. Sensitivity to fracture energy.

with the experimental observation indicating that this type of failure is due to a crack or group of cracks propagating along the *concrete–repair* interface [22]. It is the authors' opinion that the fracture energy of the *concrete–repair* interface is needed in order to accurately predict *plate-debonding* failures.

6.3. Sensitivity to tension softening

The sensitivity of the numerical solution to the modeling of the concrete tension softening was also investigated. During the simulations, bilinear and linear softening models were used, as shown in Fig. 1(b) and (c) respectively. The numerical results shown in Fig. 12 indicate that peak loads and deflections are slightly affected by the type of softening model. From a practical point of view, the effect of type of softening model appears negligible. However, the authors consider that further study is required to verify the validity of this affirmation.

6.4. Sensitivity to compression modeling

Three different models were used in this study to predict the behavior of concrete in compression (Fig. 2). The numerical results are shown in Fig. 13. Good agreement between experimental and numerical results is obtained for any of the three models. The authors found that from a practical point of view, the use of the bilinear model (model C in Fig. 2) provided adequate accuracy.

6.5. Sensitivity to angle of dilatancy

In this study, the angle of dilatancy was varied from 20° to 40°. Numerical results shown in Fig. 14 indicate two different trends. Beam A1, failing by concrete crushing, is insensitive to changes in the angle of dilatancy. In contrast, the failure mode and peak load of beam B3, failing by plate debonding, are significantly affected by the angle of dilatancy. A low angle of dilatancy ($\psi = 20°$) results in premature plate debonding. Conversely, using a high angle of dilatancy ($\psi = 40°$) results in increased peak load. Very good results are attained using an angle of dilatancy of 30°.

7. Modeling considerations

Several simplifications and assumptions were used in the models of the RC beams simulated in this study. In this section, the numerical solution is tested in order to check

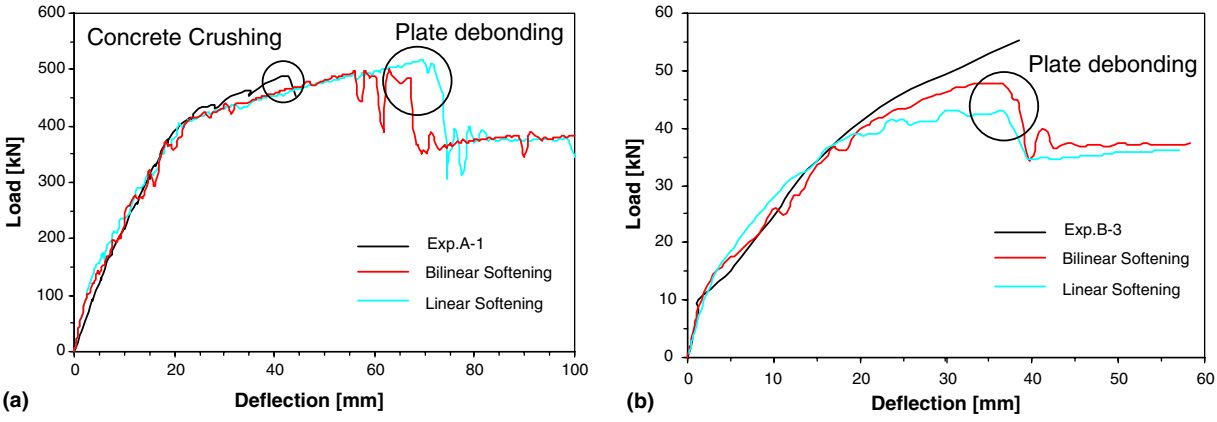

Fig. 12. Sensitivity to tension-softening model.

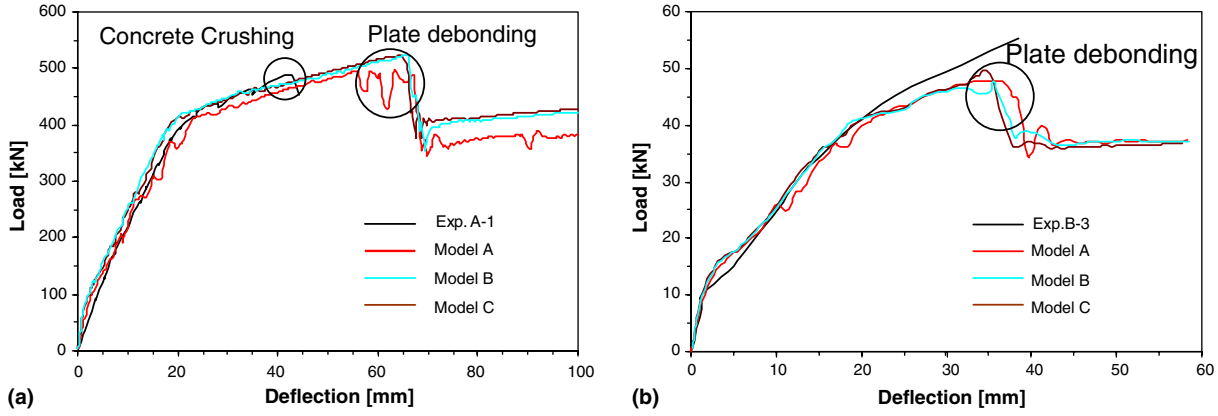

Fig. 13. Sensitivity to different compression models.

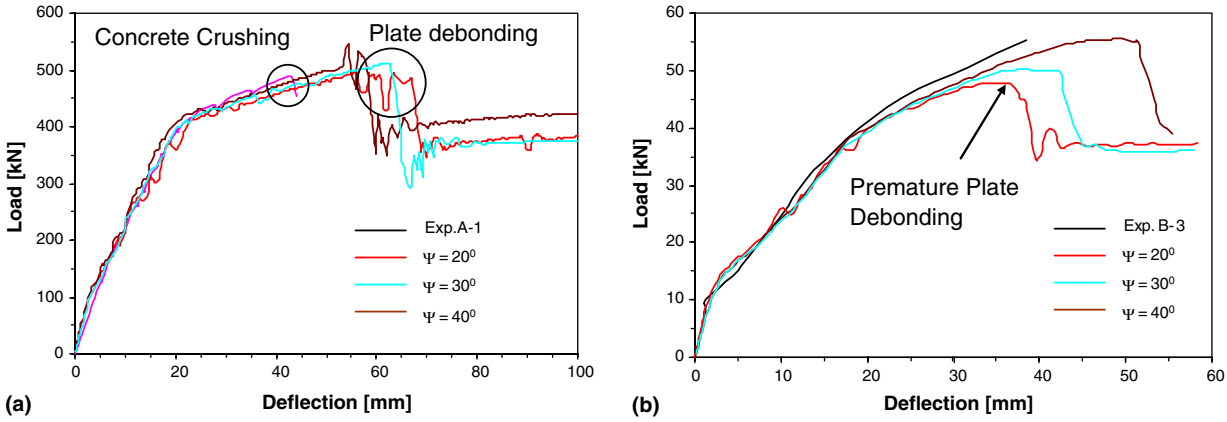

Fig. 14. Sensitivity to angle of dilatancy.

the validity of the main assumptions used during the simulation. In particular, the sensitivity to mesh size, element type and epoxy modeling is tested. Beam B3, failing by plate debonding, was selected for illustration purposes.

7.1. Mesh sensitivity

Numerical simulations must be objective. The results of the calculations made with them should not depend on subjective aspects such as the choice of mesh or element size. Three mesh configurations were used, as shown in Fig. 15. The obtained load–deflection curves are shown in Fig. 16. All three simulations predict almost identical results. Slight differences are observed in the peak loads and deflections; however, the differences are within the margin of error expected for a numerical simulation.

The results presented in this section confirm the objectivity of the numerical solution. Additionally, it is interesting to note that excellent results are obtained when the coarse mesh A is used. This can be explained by the fact that the damage processes, resulting in concrete cracking and plate debonding, involve *length scales* in the order of two to three aggregate sizes ([7, p. 227]). Therefore, adequate results can be obtained from simulations using element sizes of a similar order of magnitude.

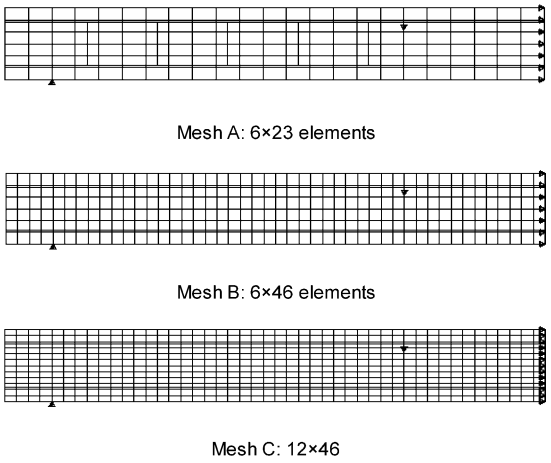

Fig. 15. Mesh configurations. Sensitivity to mesh size.

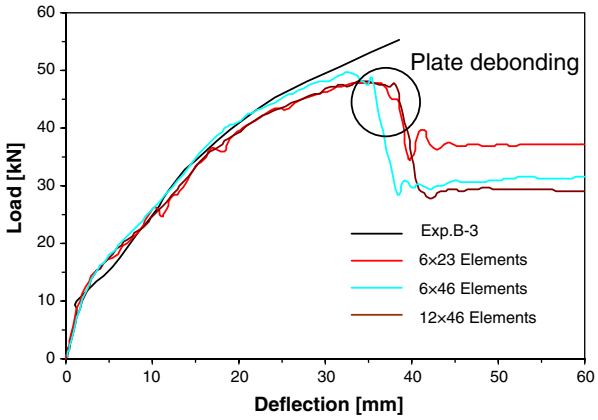

Fig. 16. Sensitivity to element size.

7.2. FRP modeling

The effect of modeling the FRP laminate using different element types is presented in Fig. 17. During the simulations, the FRP was modeled using plain strain (CPE4R) and truss (T2D2) elements. As can be seen, both approaches are capable of reproducing the global load–deflection behavior of control beam B3. The models predict slightly different failure loads and deflections. However, from a practical point of view, truss elements reduce the numerical cost of the solution, and therefore are recommended.

7.3. Concrete–epoxy interface modeling

The effect of modeling the *concrete–epoxy interface* is investigated in this section. During the numerical simulation, the epoxy and FRP were modeled using plain strain elements (CPE4R). The epoxy elements were bonded to the concrete using tied contact. In this approach, each of the nodes on the epoxy has the same displacement as the

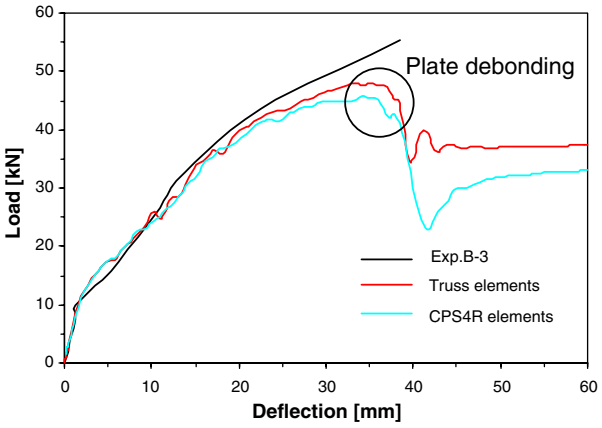

Fig. 17. Sensitivity to FRP modeling.

point on the concrete surface to which it is closest. This allows for the modeling of normal and shear stresses along the entire concrete–epoxy interface.

Numerical results are presented in Fig. 18. For comparison purposes, a model with no epoxy is also included. In this case, the FRP laminate was modeled using truss elements; in this approach, the load transfer takes place only at the connection nodes. As can be seen, both approaches are capable of reproducing the global load–deflection behavior of beam B3. The models predict slightly different failure loads and deflections. This general behavior was observed for all beams from Series A–C.

The similarity in the numerical results implies that even for beams failing by plate debonding, the modeling of the epoxy has a minor effect in the beam overall response. It is the authors' opinion that the fracture energy of the concrete–epoxy interface is the key parameter for modeling the behavior of beams failing by plate debonding. This energy controls the damage processes taking place in the concrete cover along the concrete–epoxy interface. Experimental procedures are needed to determine this energy. The use of this parameter will improve the quality of the numerical procedures presented in this study.

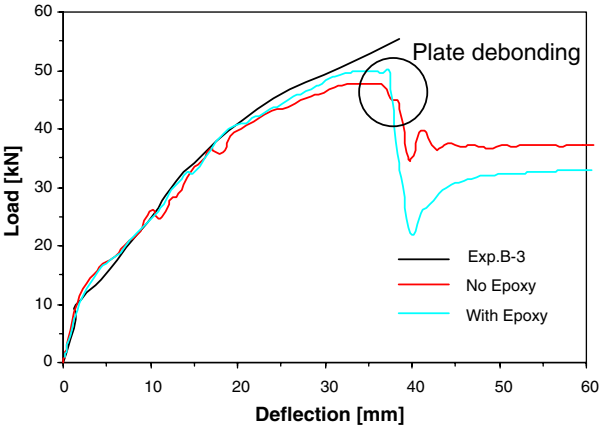

Fig. 18. Sensitivity to epoxy modeling.

8. Conclusions

The behavior of reinforced concrete beams strengthened with FRP laminates was simulated using the finite-element method (FEM). The sensitivity of the numerical results was studied. In particular, the effect of the concrete constitutive behavior and different modeling considerations was evaluated. Practical recommendations are given for the modeling of FRP, epoxy, selecting model parameters and element size. Conclusions derived from this study are as follows:

- The FEM models were capable of predicting the load–deflection behavior of both reinforced concrete (RC) beams and FRP-strengthened RC beams. The failure modes predicted (concrete crushing, plate debonding and cover failure) were the same as those obtained experimentally.
- The numerical simulations indicate that the concrete tensile strength does not constitute the unique failure criterion for predicting plate-debonding failure of strengthened RC beams.
- The fracture energy of the concrete–epoxy interface is needed to accurately predict plate-debonding failures. This finding agrees with experimental observations, indicating that this phenomenon is due to a crack propagating along the concrete–epoxy interface.
- Peak loads and deflections are slightly affected by the type of concrete softening used. From a practical point of view, these effects are negligible.
- No significant changes were observed in the global response of the CFRP-strengthened beams when different modeling approaches were used for the FRP laminate.
- The numerical results were insensitive to the mesh geometry, which demonstrates the objectivity of the modeling approach used during this study.
- The modeling of the epoxy has a minor effect in the overall response of strengthened RC beams, even for beams failing by plate debonding.

Further experimental and analytical work is currently underway to obtain the fracture energy of the *concrete–epoxy interface*.

Acknowledgement

The research activities described in this paper have been supported by a CAREER Grant from the National Science Foundation (CMS-0330592). This support is gratefully acknowledged.

References

[1] ACI 440.2R-02. Guide for the design and construction of externally bonded FRP systems for strengthening concrete structures. Reported by ACI Committee 440;2002:21–2.

[2] Ziraba YN, Baluch MH. Computational model for reinforced concrete beams strengthened by epoxy bonded steel plates. Finite Elem Anal Des 1995;20(4):253–71.
[3] Arduini M, Di Tommaso A, et al. Brittle failure in FRP plate and sheet bonded beams. ACI Struct J 1997;94(4):363–70.
[4] Wong RSY, Vecchio FJ. Towards modeling of reinforced concrete members with externally bonded fiber-reinforced polymer composites. ACI Struct J 2003;100(1):47–55.
[5] Benkert A. Study of the development length of fiber reinforced laminates used for strengthening of reinforce concrete beams. Master of Science Thesis. Clarkson University, 2002.
[6] Rahimi H, Hutchinson A. Concrete beams strengthened with externally bonded FRP plates. J Compos Constr 2001;5(1):44–56.
[7] Bazant Z. Mechanics of distributed cracking. Appl Mech Rev 1986; 39:675–705.
[8] Lubliner J, Oliver J, Oller S, Onate E. Plastic-damage model for concrete. Int J Solids Struct 1989;25(3):299–326.
[9] Lee J, Fenves LG. Plastic-damage concrete model for earthquake analysis of dams. Earthquake Eng Struct Dyn 1998;27(9): 937–56.
[10] ABAQUS/Explicit User's Manual, Version 6.3. Hibbitt, Karlson & Sorensen, Inc. Pawtucket, RI. 2002.
[11] Bazant ZP, Planas J. Fracture and size effect in concrete and other quasibrittle materials. New directions in civil engineering, vol. xxii. Boca Raton: CRC Press; 1998. p. 616.
[12] Rocco C, Guinea GV, Planas J, Elices M. Review of the splitting-test standards from a fracture mechanics point of view. Cement Concrete Res 2001;31(1):73–82.
[13] Hillerborg A. Theoretical basis of a method to determine the fracture energy G_F of concrete. Mater Struct 1985(106):291–6.
[14] Elices M, Guinea GV, Gomez J, Planas J. The cohesive zone model: advantages, limitations and challenges. Eng Fract Mech 2002;69(2): 137–63.
[15] MacGregor JG. 3rd ed. Reinforced concrete: mechanics and design, vol. xiii. Upper Saddle River, NJ: Prentice Hall; 1997. p. 939.
[16] Bazant ZP, Becq-Giraudon E. Statistical prediction of fracture parameters of concrete and implications for choice of testing standard. Cement Concrete Res 2002;32(4):529–56.
[17] ASTM C469-02. Standard test method for static modulus of elasticity and Poisson's ratio of concrete in compression. Annual book of ASTM standards, vol. 04.02.
[18] ACI 318-02. Building code requirements for structural concrete (ACI 318-02) and commentary (ACI 318R-02). Reported by ACI Committee 318;2002:18.3.3.
[19] Chen W-F. Plasticity in reinforced concrete, xv. New York: McGraw-Hill; 1982. p. 474.
[20] Naaman A, Park S, Lopez M, Till R. Parameters influencing the flexural response of RC beams strengthened using CFRP sheets. Fibre-reinforced plastics for reinforced concrete structures, vol. 1. Cambridge: Thomas Telford; 2001. p. 117–25.
[21] Malek A, Saadatmanesh H, Ehsani R. Prediction of failure load of RC beams strengthened with FRP plate due to stress concentration at the plate end. ACI Struct J 1998.
[22] Lopez MM. Study of the flexural behavior of reinforced concrete beams strengthened by externally bonded fiber reinforced polymeric (FRP) laminates. Ph.D Thesis. University of Michigan, 2000.